Journal of the Physical Society of Japan **86**, 044705 (2017)
https://doi.org/10.7566/JPSJ.86.044705

Magnetic Structure and Quadrupolar Order Parameter Driven by Geometrical Frustration Effect in NdB_4

Hiroki Yamauchi[1*], Naoto Metoki[1,2], Ryuta Watanuki[3], Kazuya Suzuki[3], Hiroshi Fukazawa[1], Songxue Chi[4], and Jaime A. Fernandez-Baca[4]

[1]*Materials Sciences Research Center, Japan Atomic Energy Agency, Tokai, Ibaraki 319-1195, Japan*
[2]*Institute of Quantum Beam Science, Ibaraki University, Tokai, Ibaraki 319-1106, Japan*
[3]*Faculty of Engineering, Yokohama National University, Yokohama 240-8501, Japan*
[4]*Quantum Condensed Matter Division, Oak Ridge National Laboratory, Oak Ridge, TN 37831-6393, U.S.A.*

(Received September 28, 2016; accepted February 2, 2017; published online March 10, 2017)

Neutron diffraction experiments have been carried out to characterize the magnetic structures and order parameters in an intermediate phase of NdB_4 showing the successive phase transitions at $T_0 = 17.2$ K, $T_{N1} = 7.0$ K, and $T_{N2} = 4.8$ K. We have revealed the antiferromagnetic ordering with the propagation vectors $\mathbf{q}_0 = (0, 0, 0)$, $\mathbf{q}_0$ and $\mathbf{q}_{s1} = (\delta, \delta, 0.4)$ ($\delta \sim 0.14$), and $\mathbf{q}_0$ and $\mathbf{q}_{s2} = (0.2, 0, 0.4)$ in phase II ($T_{N1} < T < T_0$), phase III ($T_{N2} < T < T_{N1}$), and phase IV ($T < T_{N2}$), respectively. The observed patterns in phase II are successfully explained by postulating a coplanar structure with static magnetic moments in the tetragonal *ab*-plane. We have found that the magnetic structure in phase II can be uniquely determined to be a linear combination of antiferromagnetic "all-in/all-out"-type (Γ_4) and "vortex"-type (Γ_2) structures, consisting of a Γ_4 main component (77%) with a small amplitude of Γ_2 (23%). We propose that the quadrupolar interaction holds the key to stabilizing the noncollinear magnetic structure and quadrupolar order. Here, the frustration in the Shastry–Sutherland lattice would play an essential role in suppressing the dominance of the magnetic interaction.

1. Introduction

Geometrical frustration can cause unusual quantum states, which are mostly suppressed by dominant exchange interactions. A simple magnetic long-range order (i.e., Néel state) may become energetically unfavorable or even unstable as a consequence of conflicting magnetic intersite interactions. This results in novel quantum states such as spin ice and spin liquid,[1–5] or unusual partial order in a series of successive transitions with a complicated magnetic phase diagram.[6–8] Typical examples include triangular, kagome, and pyrochlore lattices and hexagonal ATX_3 compounds (A = Rb, Cs; T = Co, Ni; and X = Cl, Br). As for $CsCoCl_3$, $CsNiBr_3$, and $CsNiCl_3$, the magnetic chains of transition metals form triangular lattices. The spin frustration among the chains realizes the successive magnetic transitions and leads to a partial disorder on triangle lattices in an intermediate phase or the ordering of the *c*- and *ab*-components at different temperatures.[6–8] The Shastry–Sutherland (SS) lattice is also one of the intriguing systems with geometrical frustration, in which the strengths of intra- and interdimer interactions can control quantum spin states.[9] $SrCu_2(BO_3)_2$ is an archetypal quantum magnet with a spin gap between a singlet-dimer ground state and a triplet, whose spin excitations show weak band dispersion due to the Dzyaloshinskii–Moriya (DM) interaction.[10–12]

A recent analog of the SS lattice has been confirmed in rare-earth tetraborides, RB_4. This series crystallizes in a tetragonal structure belonging to the space group D_{4h}^5–$P4/mbm$ except for R = Pm and Eu, and is isostructural to ThB_4.[13,14] Figure 1 shows the crystal structure of RB_4. The R sublattices in the *ab*-plane form an array paved by squares and triangles, which is topologically equivalent to the SS lattice. The thick lines in the ⟨110⟩ directions correspond to the SS dimers with the nearest-neighbor coupling. The dashed thin lines represent the second nearest neighbors. The R atoms also lie at the top and bottom of the center of seven-membered rings consisting of B2 and B3 borons. The R sites have orthorhombic C_{2v} symmetry.

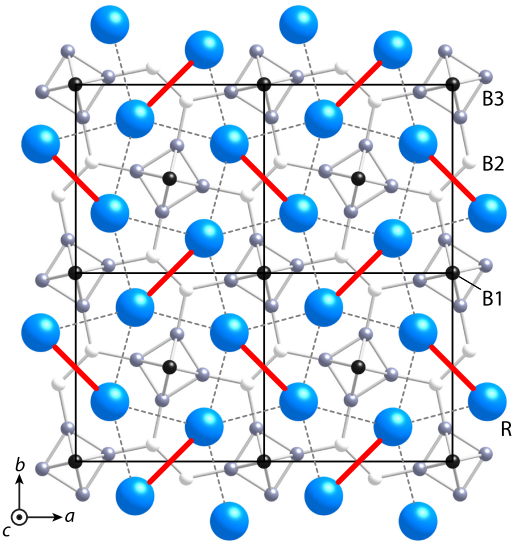

Fig. 1. (Color online) Projection view of the crystal structure of RB_4 onto the *ab*-plane. The large spheres correspond to R atoms, lying in the $z = 0$ plane. The small black, white, and gray spheres correspond to boron B1, B2, and B3 atoms, respectively. The B1 and B3 atoms form octahedra. The B2 and B3 atoms form seven-membered rings in the $z = 0.5$ plane. The thick lines in the ⟨110⟩ directions denote the Shastry–Sutherland dimers with the nearest-neighbor coupling. The dashed thin lines represent the second nearest neighbors.

Note that many of RB_4 (R = Tb, Dy, Ho, Tm, Pr, Nd, and Sm) show successive magnetic transitions.[15–18] Moreover, most of RB_4 exhibit antiferromagnetic transition(s) apart from paramagnetic CeB_4 and YbB_4.[19,20] The emerging magnetic order parameter in the RB_4 family is attributed to the localized nature of 4*f* electrons with large effective moments interacting via the Ruderman–Kittel–Kasuya–Yoshida (RKKY) interaction. Recently, the existence of

unusual magnetic successive transitions with the fractional magnetization plateaus of TbB_4 and TmB_4 has attracted interest.[21–26] In particular, the successive transitions in DyB_4 and HoB_4, which are accompanied by a partial magnetic order coupled to a quadrupole order parameter, have been studied extensively.[27–30]

NdB_4 has also been found to exhibit successive phase transitions at $T_0 = 17.2$ K, $T_{N1} = 7.0$ K, and $T_{N2} = 4.8$ K.[17] In the previous study involving magnetic susceptibility and specific heat measurements, the zero-field magnetic phases are established as follows: paramagnetic phase I ($T > T_0$), phase II ($T_{N1} < T < T_0$), phase III ($T_{N2} < T < T_{N1}$), and phase IV ($T < T_{N2}$). The specific heat shows two λ-type anomalies at T_{N1} and T_0, and a first-order-like anomaly at T_{N2}. The magnetic entropy of $R \ln 2$ and $R \ln 4$ is released approximately at T_{N1} and T_0, respectively, indicating that the ground state of the crystalline electric field (CEF) is a pseudo-quartet consisting of two Kramers doublets. This pseudo-quartet carries the magnetic dipole and electric quadrupole degrees of freedom. The magnetic susceptibility for the easy c-direction exhibits clear antiferromagnetic anomalies at T_{N1} and T_{N2}. It is notable that only the susceptibility within the ab-plane exhibits a tiny cusp anomaly at T_0. Additionally, no spontaneous magnetization is observed. These results can allow us to interpret that the c- and ab-components of the magnetic moments of Nd^{3+} ions order independently at different temperatures. Nevertheless, the ordered state (especially in phase II) of NdB_4 has not been identified yet.

In this work, we focus on the magnetic structures and effects of geometrical frustration in NdB_4. We have performed neutron diffraction experiments and have determined the magnetic structure of phase II. We discuss multipolar order parameters and the role of geometrical frustration on the basis of the magnetic structure which has not been found in the other RB_4 compounds.

2. Experimental Procedure

High-quality NdB_4 single crystals were grown by the floating zone method in a four-ellipsoidal mirror-type image furnace. The ^{11}B isotope enriched to 99.5% was used wherever possible to keep away from the strong neutron absorption of ^{10}B contained in natural boron. A polycrystalline powder sample of 7.1 g was prepared by crushing the single crystals. A rectangular single crystal with dimensions of $4 \times 2 \times 2$ mm^3 was used in single-crystal experiments.

Neutron powder diffraction data were collected on the wide-angle neutron diffractometer WAND (HB-2C) installed at the High Flux Isotope Reactor (HFIR) in the Oak Ridge National Laboratory (ORNL), U.S.A. An incident neutron beam of 1.4827 Å wavelength was obtained from a Ge(113) monochromator. The diffraction patterns were analyzed by the Rietveld refinement method with the software FullProf.[31] Representational analysis was employed using the software SARAh to deduce symmetry-allowed magnetic structures that were constrained with the crystallographic symmetry at the paramagnetic state and the propagation vector(s) of the magnetic ordering.[32,33] A part of the crystal and magnetic structures was drawn with the aid of the software VESTA.[34]

To avoid the strong multiple scattering in NdB_4, neutron single-crystal diffraction experiments were carried out using long-wavelength neutrons on the cold neutron triple-axis spectrometer LTAS (C2-1) installed at the research reactor JRR-3 in the Japan Atomic Energy Agency (JAEA). Incident neutrons of 4.8332 Å wavelength were generated by the PG(002) reflection of the pyrolytic graphite monochromator. The higher-order contaminations were removed using a cooled Be filter placed in front of the sample. The horizontal collimation was set in the condition of (guide)–80′–80′–(open).

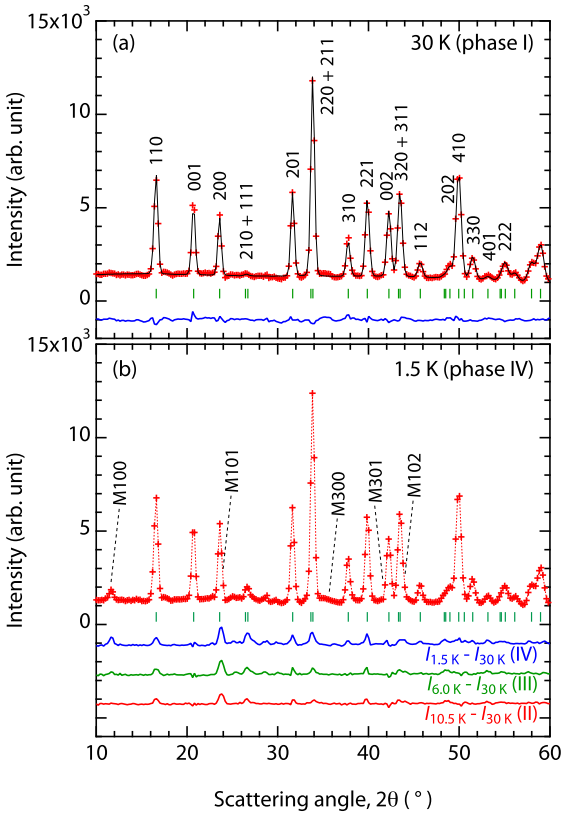

Fig. 2. (Color online) Neutron powder diffraction patterns for (a) phase I at 30 K and (b) phase IV at 1.5 K of NdB_4. The plus marks and dotted lines are the observed patterns. The thin solid line in (a) is the calculated powder pattern. Difference between the observed and calculated patterns is plotted in (a) as the thick solid line. Vertical bars represent the calculated positions of the nuclear peaks. The thermal evolutions of magnetic reflections at 1.5 K, 6.0 K (phase III), and 10.5 K (phase II) are obtained by subtracting the pattern at 30 K and shown concurrently in (b) as the thick solid lines.

3. Results

3.1 Neutron diffraction experiments

Figure 2 shows neutron powder diffraction patterns of NdB_4 measured at (a) 30 K in the paramagnetic phase I and (b) 1.5 K in the lowest-temperature phase IV. The intensity variations of the diffraction patterns in phases II, III, and IV are also shown in Fig. 2(b) as differences with the diffraction pattern at 30 K. As shown in Fig. 2(a), the crystal structure at 30 K was refined by the conventional Rietveld method and well explained with the tetragonal structure published previously with the space group $P4/mbm$. Crystallographic sites of atoms in NdB_4 are as follows: Nd ($4g$: $x, x + 0.5, 0$), B1 ($4e$: $0, 0, z$), B2 ($4h$: $x, x + 0.5, 0.5$), and B3 ($8j$: $x, y, 0.5$). A summary of the obtained parameters and the reliability factors are listed in Table I. However, the isotropic atomic displacement parameters B_{iso} were fixed to $B_{iso}(\mathrm{Nd}) = 0.4$ Å^2

Table I. Crystallographic parameters and reliability factors (*R*-factors) obtained from the Rietveld refinement for NdB_4 at 30 K.

Atom	Site	x	y	z
Nd	4*g*	0.3180(5)	$= x + 0.5$	0
B1	4*e*	0	0	0.2071(11)
B2	4*h*	0.0881(5)	$= x + 0.5$	0.5
B3	8*j*	0.1728(5)	0.0362(6)	0.5

$a = b = 7.2346(3)$ Å, $c = 4.1101(3)$ Å

$R_{wp} = 8.45\%$, $R_{exp} = 4.91\%$, $R_{Bragg} = 4.44\%$, $\chi^2 = (R_{wp}/R_{exp})^2 = 2.96$

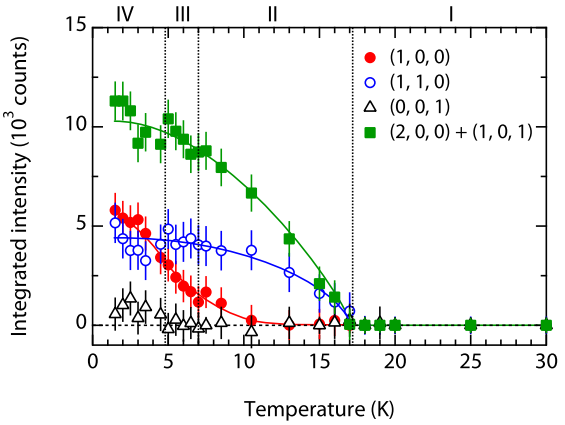

Fig. 3. (Color online) Temperature dependence of the integrated intensities of magnetic $(1,0,0)$, $(1,1,0)$, $(0,0,1)$, and $(2,0,0)+(1,0,1)$ reflections obtained from the neutron powder diffraction experiments. The solid lines are guides to the eye.

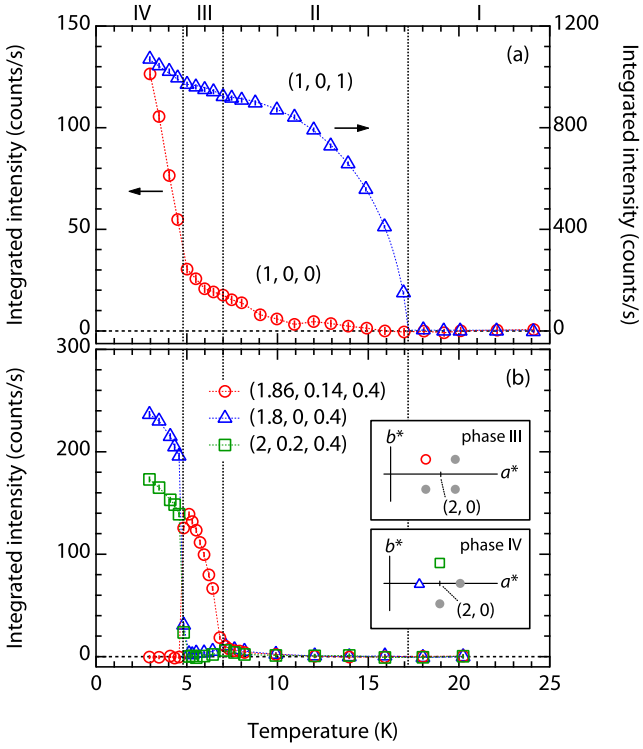

Fig. 4. (Color online) Temperature dependence of the integrated intensities of some magnetic reflections measured by the neutron single-crystal diffraction experiments: (a) commensurate $(1,0,0)$ and $(1,0,1)$ reflections, and (b) satellite $(1.86,0.14,0.4)$, $(1.8,0,0.4)$, and $(2,0.2,0.4)$ reflections. The insets show the measured satellite positions in the $(h,k,0.4)$ plane.

and $B_{iso}(B1) = B_{iso}(B2) = B_{iso}(B3) = 0.15$ Å^2 during all analyses.

In phase II, the growths of the integer *hkl* reflections are observed, which includes the forbidden reflections $h00$ (h = odd) and $0kl$ (k = odd), indicating the existence of an antiferromagnetic order with the propagation vector $\mathbf{q}_0 = (0,0,0)$. In phases III and IV, weak satellite reflections are observed, for example, at around $2\theta = 25$ and 29° as shown in Fig. 2(b) in addition to the increases in the magnetic reflections with $\mathbf{q}_0$. Figure 3 shows the temperature dependence of the integrated intensities of magnetic $(1,0,0)$, $(1,1,0)$, $(0,0,1)$, and $(2,0,0)+(1,0,1)$ reflections. The magnetic $(1,1,0)$ and $(2,0,0)+(1,0,1)$ reflections emerge clearly below T_0 and show increases related to the primary order parameter with decreasing temperature. In contrast, note that the magnetic $(1,0,0)$ reflection is of the induced type; the $(1,0,0)$ intensity is not recognized in the vicinity of T_0 within the experimental accuracy and gradually develops below the temperature (around 10 K) much less than T_0.

The propagation vectors of the magnetic structures in phases III and IV were determined by neutron single-crystal diffraction experiments. Figure 4 shows the temperature dependence of the integrated intensities at (a) commensurate $(1,0,0)$ and $(1,0,1)$ positions, and (b) satellite $(1.86,0.14,0.4)$, $(1.8,0,0.4)$, and $(2,0.2,0.4)$ positions. The onsets of phase transitions derived from the integrated intensities are well-marked and in good agreement with macroscopic properties in a previous study.[17)]

As well as in the polycrystalline measurements, the $(1,0,0)$ reflection is not observable just below T_0 within the experimental accuracy. The $(1,0,0)$ intensity increases gradually with decreasing temperature, and grows abruptly below T_{N2}. The magnetic $(1,0,1)$ reflection exhibits an order-parameter-like increase below T_0. With decreasing temperature, the satellite $(1.86,0.14,0.4)$ emerges below T_{N1} and vanishes suddenly at T_{N2}, while the satellite $(1.8,0,0.4)$ and $(2,0.2,0.4)$ intensities jump up below T_{N2}.

Consequently, our diffraction experiments on a single-crystal sample could bring out the antiferromagnetic ordering with $\mathbf{q}_0 = (0,0,0)$, $\mathbf{q}_0$ and $\mathbf{q}_{s1} = (\delta,\delta,0.4)$ where $\delta \sim 0.14$, and $\mathbf{q}_0$ and $\mathbf{q}_{s2} = (0.2,0,0.4)$ for phases II, III, and IV, respectively. The satellite reflections at around $2\theta = 25$ and 29° in the powder diffraction experiments were also explained well within the instrumental resolution by $(2,0,1) - \mathbf{q}_{s1}$ (or $\mathbf{q}_{s2}$) and $(0,0,1) + \mathbf{q}_{s1}$ (or $\mathbf{q}_{s2}$), respectively.

3.2 *Model construction of magnetic structure in phase II*

Figure 5 shows the symmetry-allowed 12 magnetic structure models in phase II given as basis vectors of irreducible representation for the Nd 4*g* site in the space group $P4/mbm$ with $\mathbf{q}_0 = (0,0,0)$. The Landau theory of second-order phase transitions states that only one representation can be involved in a critical transition. We therefore chose the basis vectors of the irreducible representations Γ_2, Γ_4, Γ_6, and Γ_8 as the candidate for a magnetic structure model in phase II. This choice was made under the following conditions for the magnetic moments $\mathbf{m}_i$ from existing experimental results and our hypotheses:

(1) no ferromagnetic moment ($\sum_i^{\text{unit cell}} \mathbf{m}_i = 0$);
(2) the planer magnetic moments $\mathbf{m}_i$ in the *ab*-plane; and
(3) the same $|\mathbf{m}_i|$ for all Nd sites.

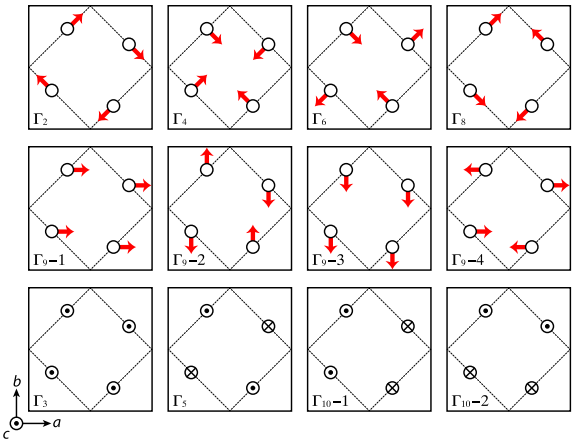

Fig. 5. (Color online) Decomposed sets in terms of the irreducible representations Γ_ν and the associated basis vectors of the Nd $4g$ site in the space group $P4/mbm$ with $\mathbf{q}_0 = (0, 0, 0)$ calculated using the software SARA*h*.[32,33]

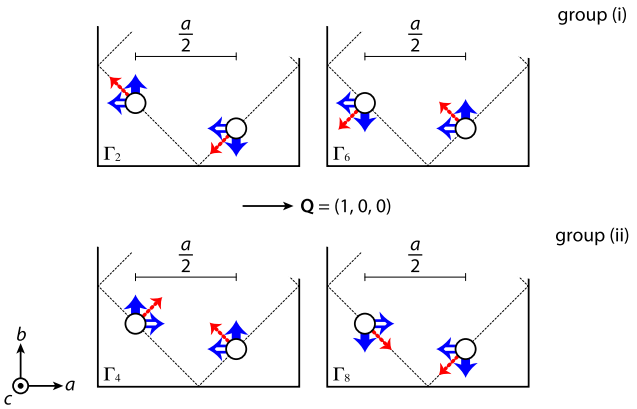

Fig. 6. (Color online) Grouping of the possible structure models Γ_2, Γ_4, Γ_6, and Γ_8 by the magnetic alignments of the longitudinal a-component (thick open arrows) and transverse b-component (thick filled arrows) of magnetic moments in a pair with the displacement of a half unit cell along the a-axis. Group (i) indicates that the a- and b-components are ferromagnetic and antiferromagnetic, respectively, while vice versa in group (ii).

At first, we can immediately rule out the planar Γ_9-1 and Γ_9-3 models and the axial Γ_3, Γ_5, and Γ_{10} models due to conditions (1) and (2). Secondly, the in-plane collinear Γ_9-2 and Γ_9-4 models cannot explain the diffraction data. The mixing of these collinear structures with noncollinear structures Γ_2, Γ_4, Γ_6, or Γ_8 does not satisfy condition (3). Moreover, almost all RB_4 (R = Gd,[35] Tb,[36] Dy,[28] Ho,[29] Er[37]) have antiferromagnetic correlations in SS dimer bonds except for TmB_4 with axial magnetic structures along the c-axis.[24,25] Therefore, we consider that it is reasonable to set aside Γ_9 representations with ferromagnetically coupled dimer bonds at an early stage.

The remaining four noncollinear structures are characterized by the arrangement of the local moments in a unit cell: "vortex" (Γ_2), "two-in two-out" (Γ_6), "all-in/all-out" (Γ_4), and "rhombus" (Γ_8), where all the magnetic moments are parallel to the $\langle 110 \rangle$ diagonal directions. The angle between two magnetic moments is 90° in a pair with the displacement of a half unit cell along the a-axis (and also along the b-axis). Thus, the magnetic moments are described as a superposition of ferromagnetic (FM) and antiferromagnetic (AFM) modulations. The four structures can be classified into two groups according to the modulations:

(i) Γ_2 and Γ_6 with longitudinal FM and transverse AFM modulations; and
(ii) Γ_4 and Γ_8 with longitudinal AFM and transverse FM modulations.

The "longitudinal" and "transverse" here denote the modulation parallel and perpendicular to the reciprocal vector along the a^*-axis, respectively. For example, Fig. 6 shows the magnetic modulations of a pair separated by the distance $a/2$ along the a-axis. In group (i), the longitudinal a-components (open arrows) are FM, while the transverse b-components (filled arrows) are AFM, and vice versa in group (ii). Since the transverse component of $\mathbf{m}_i$ perpendicular to the scattering vector $\mathbf{Q}$ contributes the magnetic neutron scattering amplitude, no scattering cross section exists for the longitudinal component of $\mathbf{m}_i$. Therefore, the $(1, 0, 0)$ reflection, which is forbidden by the crystal symmetry, can be expected in group (i) with the transverse AFM modulation, while it is absent in group (ii) with the longitudinal AFM modulation.

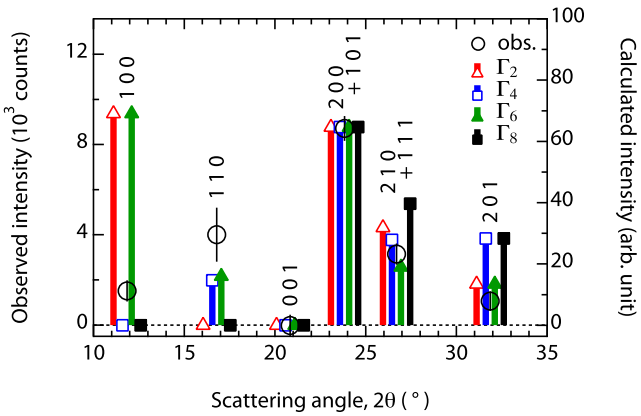

Fig. 7. (Color online) Comparison between the observed intensities (circles) of the magnetic reflections in the powder data at 7.5 K and the calculated ones (triangles and squares with bars) for the basis vectors Γ_2, Γ_4, Γ_6, and Γ_8 below $2\theta = 33°$. Both intensities are normalized at the intense $(1, 0, 1)$ reflection.

The $(1, 1, 0)$ reflection can be considered in a similar manner, and the calculations of magnetic structure factors indicate that both the $(1, 0, 0)$ and $(1, 1, 0)$ intensities are important to distinguish the remaining four structures. The bars in Fig. 7 show the calculated result of the polycrystalline averaged intensities for the basis magnetic structures of Γ_2, Γ_4, Γ_6, and Γ_8 with the experimental data obtained in phase II at 7.5 K. The intensities of nuclear reflections and background in the paramagnetic phase at 30 K are subtracted from the experimental data. The observed and calculated data were normalized at the intense $(1, 0, 1)$ reflection. The calculated $(1, 0, 0)$ and $(1, 1, 0)$ intensities are listed in Table II for easier comparison.

The following considerations lead us to conclude that the Γ_4 structure is the main component in phase II. We observed experimentally both the $(1, 0, 0)$ and $(1, 1, 0)$ reflections, but there are remarkable discrepancies in the emergence of the $(1, 0, 0)$ and $(1, 1, 0)$ reflections. The intensity of the $(1, 0, 0)$ reflection is very weak, and does not show the temperature dependence of a primary order parameter but of the induced type, as can be seen in Figs. 3 and 4. Therefore, the Γ_2 and

Table II. Extracted list of the calculated 100 and 110 intensities in arbitrary unit for the Γ_2, Γ_4, Γ_6, and Γ_8 structures.

	Γ_2	Γ_4	Γ_6	Γ_8
$I_{cal}(100)$	63.4	0	63.4	0
$I_{cal}(110)$	0	14.7	14.7	0

Γ_6 structures in group (i), which are accompanied by the strong $(1,0,0)$ reflection, are not definitely the main component. Meanwhile, the $(1,1,0)$ reflection is conspicuous and its temperature dependence reflects the primary order parameter as shown in Fig. 3, but the Γ_8 structure in group (ii) does not involve the $(1,1,0)$ reflection at all, as shown in Fig. 7 and Table II. As a result, we concluded that the Γ_4 structure should be the main component and we tried to explain the discrepancy from the experimental results, especially the existence of the weakly induced $(1,0,0)$ reflection, by mixing with the other three structures Γ_2, Γ_6, and Γ_8 as a minor component.

We have subsequently found that the mixing of Γ_2 into Γ_4 (henceforth expressed as $\Gamma_4+\Gamma_2$ or $\Gamma_4-\Gamma_2$), namely, the structure consisting of a Γ_4 main component with a small amplitude of Γ_2, was the unique structure model in phase II of NdB_4. The microscopic mixing of $\Gamma_4+\Gamma_2$ is equivalent to the rotation of magnetic moments from the $\langle 110\rangle$ directions with the angle φ in the *ab*-plane, which corresponds to a linear combination of Γ_4 and Γ_2. The intensity of $(1,0,0)$ increases with increasing Γ_2 component, in other words, with the increase in the transverse antiferromagnetic component accompanied by a rotation of the Γ_4 arrangement with φ.

The case of $\Gamma_4+\Gamma_6$ can be immediately ruled out because the magnetic moments with two different sizes are generated after mixing. This is not allowed by the previously described condition (3). The magnetic moment at each site in Γ_6 is either parallel or antiparallel to that at the same site for Γ_4. As a consequence of the mixing, the magnetic moments increase at the parallel sites or decrease at the antiparallel sites.

It is easily understood that $\Gamma_4+\Gamma_8$ is equivalent to the rotation $\pm\varphi$ of magnetic moments in the *ab*-plane, where the sign depends on the Nd site. Therefore, the moment size remains the same for all sites. However, we do not expect the emergence of the $(1,0,0)$ reflection in $\Gamma_4+\Gamma_8$ since each component of Γ_4 and Γ_8 has only longitudinal AFM modulation, which does not contribute to the magnetic neutron scattering amplitude.

Finally, the combinations of three basis structures including Γ_4 are not appropriate because the forbidden pair of either $\Gamma_4+\Gamma_6$ or $\Gamma_2+\Gamma_8$ is surely included in those combinations. $\Gamma_2+\Gamma_8$ is also the case that the magnitudes of magnetic moments are not the same for all sites. The mixing of all four structures is also excluded because of the same reason.

Since it is impossible to distinguish between the microscopic and macroscopic mixings by the nonpolarized neutron powder experiments, the macroscopic coexistence with the Γ_4 and Γ_2 domains cannot be ruled out at this stage. However, we have observed simple CEF excitations below 6 meV at the lowest temperature by inelastic neutron scattering experiments, indicating that the Nd^{3+} ions in the ordered states are uniform and of single site. Therefore, we consider that a microscopic mixing, rather than a macroscopic one, of Γ_4 and Γ_2 is very likely.

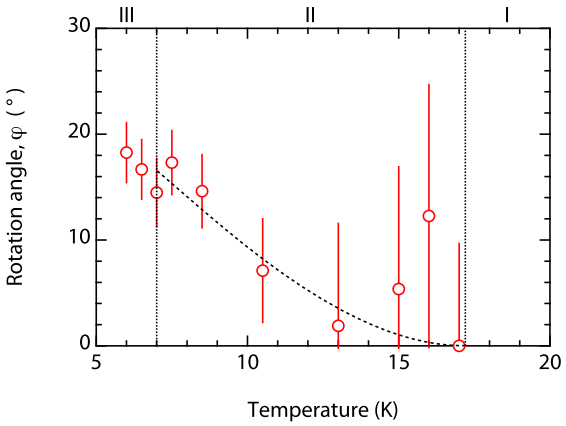

Fig. 8. (Color online) Temperature dependence of the rotation angle φ of the magnetic moments from the $\langle 110\rangle$ directions in the *ab*-plane below T_0. The dashed line is a guide to the eye.

We have preliminarily estimated that $A_{\Gamma_2}/A_{\Gamma_4}\simeq 1/3$ is in good agreement with the intensities of magnetic reflections observed at 7.5 K, where A_{Γ_2} and A_{Γ_4} denote the amplitudes (magnetic moments) of Γ_2 and Γ_4, respectively. This agreement is also recognized as experimental evidence that the *c*-component of the magnetic moment is negligibly small in phase II, and is consistent with the component-separated ordering of the magnetic moment on the *ab*-plane proposed from the magnetic susceptibility measurements.[17] The $\tan\varphi$, namely, $A_{\Gamma_2}/A_{\Gamma_4}$, can be estimated from the intensity ratio I_{100}/I_{110} as

$$\tan\varphi=\frac{A_{\Gamma_2}}{A_{\Gamma_4}}=|\cos(2\pi x)|\sqrt{2\frac{I_{100}/[(f_{100})^2L_{100}]}{I_{110}/[(f_{110})^2L_{110}]}},$$

where $x=0.318$ is the coordinate parameter for the Nd atom, f_{hkl} is the magnetic form factor, and L_{hkl} is the Lorentz factor for given indices. This simple relation is easily derived from the analytical expression of the magnetic structure factors simplified by the fact that the $(1,0,0)$ and $(1,1,0)$ reflections arise from only Γ_2 and Γ_4 structures, respectively. Figure 8 shows the temperature dependence of the rotation angle φ in phase II when the microscopic mixing of the Γ_4 and Γ_2 structures occurs. We have found that φ is nearly zero at T_0, indicating magnetic moments in the $\langle 110\rangle$ diagonal directions. This fact corresponds to the critical behavior of the single irreducible representation Γ_4 near the second-order transition temperature T_0, and is consistent with the Landau theory. With decreasing temperature, φ increases gradually up to slightly over 17° at T_{N1}. The temperature variation of φ can be reasonably understood from the difference in the temperature dependence of I_{100} from that of I_{110}, which means that the intensity ratio I_{100}/I_{110} is not constant in phase II.

3.3 *Magnetic structure refinements*

We refined the magnetic structure for phase II by Rietveld least-squares fitting of powder patterns. First of all, the magnetic structure at 10.5 K could be refined with the Γ_4 structure alone, being attributed to the negligibly small Γ_2 component within experimental error. Figure 9(a) shows the observed (plus marks), calculated (thin solid line), and those difference (thick solid line) profiles. The upper and lower vertical bars indicate the positions of the nuclear and

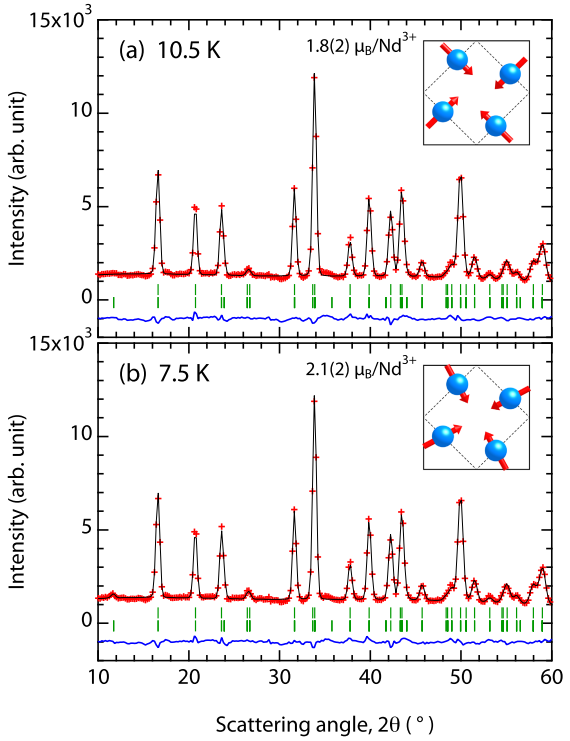

Fig. 9. (Color online) A result of the Rietveld analysis and obtained magnetic structure for phase II at (a) 10.5 K and (b) 7.5 K. The magnetic structures are schematically shown only in the *ab*-plane.

Table III. Refined structural parameters, magnetic moments, and reliability factors for NdB_4 at (a) 10.5 K (Γ_4 structure) and (b) 7.5 K ($0.77\Gamma_4 - 0.23\Gamma_2$ structure).

(a)

Atom	Site	x	y	z
Nd	4*g*	0.3177(5)	$= x + 0.5$	0
B1	4*e*	0	0	0.2064(11)
B2	4*h*	0.0884(5)	$= x + 0.5$	0.5
B3	8*j*	0.1731(5)	0.0362(6)	0.5

$a = b = 7.2351(3)$ Å, $c = 4.1099(3)$ Å, $|\mathbf{m}_{Nd}| = 1.8(2)\,\mu_B$
$R_{wp} = 8.90\%$, $R_{exp} = 4.72\%$, $R_{Bragg} = 4.56\%$, $R_{magn} = 10.5\%$, $\chi^2 = 3.56$

(b)

Atom	Site	x	y	z
Nd	4*g*	0.3180(5)	$= x + 0.5$	0
B1	4*e*	0	0	0.2071(11)
B2	4*h*	0.0881(5)	$= x + 0.5$	0.5
B3	8*j*	0.1728(5)	0.0362(6)	0.5

$a = b = 7.2349(3)$ Å, $c = 4.1101(3)$ Å, $|\mathbf{m}_{Nd}| = 2.1(2)\,\mu_B$
$R_{wp} = 8.84\%$, $R_{exp} = 4.76\%$, $R_{Bragg} = 4.21\%$, $R_{magn} = 11.3\%$, $\chi^2 = 3.45$

magnetic Bragg reflections, respectively. The obtained structural parameters, magnetic moments, and reliability factors are given in Table III(a). After that, we carried out the magnetic structure refinement with the $\Gamma_4 - \Gamma_2$ model using the data at 7.5 K. As shown in Fig. 9(b), the observed diffraction pattern at 7.5 K is well reproduced by our model calculation and the reliability factors are satisfactorily small. The refined parameters, magnetic moments, and reliability factors at 7.5 K are summarized in Table III(b). The ratio of each component in the magnetic structure was approximately $\Gamma_4 : \Gamma_2 = 1.98(8)\,\mu_B : 0.60(7)\,\mu_B$. Therefore, the magnitude of the total magnetic moment was evaluated to be $2.1(2)\,\mu_B$ at 7.5 K. Since phase II is not a ground state but a high-temperature phase and there are CEF effects acting on Nd^{3+} ions in tetragonal symmetry, the resultant magnitude $2.1(2)\,\mu_B$ of the magnetic moment is reasonably sufficient in phase II compared with the full moment of $3.62\,\mu_B$ for the free Nd^{3+} ion. Moreover, it is also expected that the *c*-component of the magnetic moments will emerge at lower temperatures. Therefore, a larger magnetic moment can develop in the lowest temperature phase.

As shown schematically in the inset of Fig. 9(b), all the magnetic moments $\mathbf{m}_{Nd}$ point almost to the center of the unit cell with the rotation of $\varphi = 16.9°$ for $\Gamma_4 - \Gamma_2$. This result suggests the rotation of the 4*f* orbital coupled with magnetic moments via spin–orbit interaction. By the way, the two structures $\Gamma_4 \pm \Gamma_2$ are different. However, we could not differentiate the two structures by means of powder diffraction. For this purpose, a polarized neutron experiment on a single domain sample is necessary.

As for phases III and IV in NdB_4, although we have some candidates for magnetic structures, the final structures have not been determined yet. The magnetic susceptibility data suggest the order of the magnetic *c*-component $\langle J_z \rangle$ below T_{N1}, which should therefore be accompanied by the incommensurate modulation with $\mathbf{q}_{s1}$ and probably maintained also in phase IV with $\mathbf{q}_{s2}$. These incommensurate modulations coexisting with $\mathbf{q}_0$ become the source of many magnetic reflections. However, the limited resolution and magnetic signal-to-background ratio were insufficient.

The intensity of antiferromagnetic reflections with $\mathbf{q}_0$ exhibits no significant change at T_{N1} as shown in Figs. 3 and 4. Therefore, we consider that the $\Gamma_4 - \Gamma_2$ structure remains stable in phase III. In this case, the incommensurate modulation $\mathbf{q}_{s1}$ of the *c*-component will correspond to the order parameter of the second-order transition at T_{N1}. In phase IV, however, we observed a remarkable increase in the $(1, 0, 0)$ reflection and a small upturn of the $(1, 0, 1)$ reflection below T_{N2}. This may be interpreted with a significant increase in the Γ_2 component, or may indicate a marked change in the magnetic structure for $\mathbf{q}_0$ modulation. Since the transition at T_{N2} is of first order, any combination without ferromagnetic components (Γ_3, Γ_9-1, and Γ_9-3) will be allowed from the group theoretical viewpoint. When the *c*-component exists also for $\mathbf{q}_0$ modulation, we expect either Γ_5 or Γ_{10}, or those mixing. These components can be separately clarified by neutron spin polarization analysis.

4. Discussion

In phase II of NdB_4, the antiferromagnetic ordering characterized as a noncollinear arrangement was reproduced mainly by the "all-in/all-out"-type Γ_4 structure as shown in Fig. 10. The magnetic moments in the *ab*-plane are almost parallel to the $\langle 110 \rangle$ diagonal axes, involving $\langle J_x \rangle$ and $\langle J_y \rangle$ as static and finite magnetic order parameters. We consider a possible scenario for this type of antiferromagnetic order parameter based on the geometrical frustration effect.

The two-dimensional Nd lattice can be regarded as the SS lattice, which produces frustration among the orthogonal dimers when the intradimer coupling is antiferromagnetic. Actually, the nearest-neighbor (intradimer) coupling of magnetic moments is antiparallel in Γ_2, Γ_4, Γ_6, and Γ_8

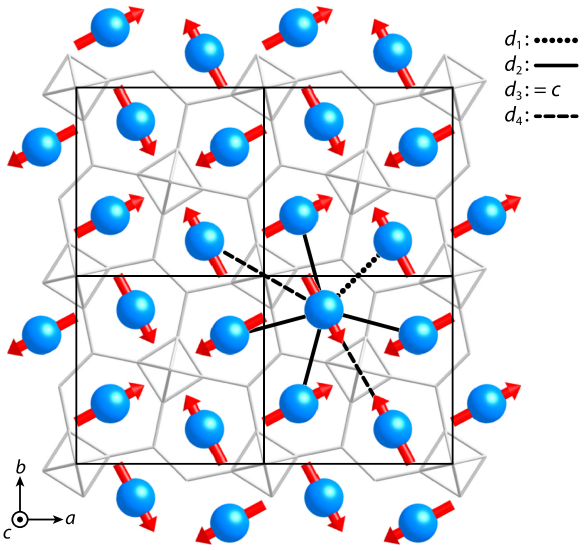

Fig. 10. (Color online) Magnetic structure in phase II of NdB_4. The lines corresponding to d_1, d_2, and d_4 represent the first, second, and fourth nearest neighbors, respectively. The third nearest neighbors are equal to the lattice constant c.

structures. Moreover, the couplings of local moments between orthogonal dimers maintain energetic equivalence with two bonds of second-nearest-neighbor (interdimer) coupling. Even in the magnetically ordered phase II, the crystal structure remains stable, thus the frustration survives. Accordingly, these noncollinear structures have the same exchange energy including the biquadratic term, which is a consequence of the frustration in the SS lattice.

The magnetic dipolar interaction also cannot be a driving force of the Γ_4 "all-in/all-out" structure. For example, it can be understood that the general dipolar interaction energy in the Γ_2 "vortex" structure is much smaller than that in the Γ_4 "all-in/all-out" structure. We roughly calculated the interaction energies for the four structures. The classical dipole pair energy between the two dipoles $\boldsymbol{\sigma}_i$ and $\boldsymbol{\sigma}_j$ separated by the vector $\mathbf{r}_{ij}$ connecting site i to site j can be expressed as:

$$\mathcal{E}_{\mathrm{dd}} = \frac{\mu_0}{4\pi} \sum_{i \neq j} \left\{ \frac{\boldsymbol{\sigma}_i \cdot \boldsymbol{\sigma}_j}{|\mathbf{r}_{ij}|^3} - 3 \frac{(\boldsymbol{\sigma}_i \cdot \mathbf{r}_{ij})(\boldsymbol{\sigma}_j \cdot \mathbf{r}_{ij})}{|\mathbf{r}_{ij}|^5} \right\},$$

where μ_0 is the vacuum permeability. The summation is for all dipole pairs on the lattice, however, counting each dipole pair only once. For simplicity, the calculation was performed for sixteen Nd atoms in the four unit cells up to the fourth nearest neighbors (NNs) as shown in Fig. 10 and as $\boldsymbol{\sigma}_i = 1\,\mu_{\mathrm{B}}$. The numbers of the NN, second NN, third NN, and fourth NN bonds for sixteen Nd atoms are 12, 40, 32, and 22, respectively. The n-th NN distances d_n and the direction vectors $\mathbf{r}_{ij}$ were estimated from the structural analysis at 7.5 K. As a result, the magnitude relation of the interaction energy $\mathcal{E}_{\mathrm{dd}}/k_{\mathrm{B}}$ was $\Gamma_6(-0.305\,\mathrm{K}) \sim \Gamma_2(-0.108\,\mathrm{K}) < \Gamma_4(0.919\,\mathrm{K}) \sim \Gamma_8(1.12\,\mathrm{K})$, where k_{B} is the Boltzmann constant.

Here, we consider that the quadrupole may play an important role, since NdB_4 has a pseudo-quartet ground state composed of two Kramers doublets with different orbitals. NdB_4 is a dipole-quadrupole coupled system, and thus the quadrupole should be somehow ordered and responsible for the successive transitions. Actually, this is consistent with the result of the heat capacity measurement and the magnetic entropy. We further consider that the quadrupolar interaction would be an origin of the "all-in/all-out"-type magnetic structure where magnetic moments are perpendicular to the long axis of seven-membered boron rings. This situation will be favorable for the $\langle O_{xy} \rangle$ electric quadrupole in the ab-plane, which is probably subject to local crystal field anisotropy. Therefore, we propose that the Γ_4 structure is attributed to the quadrupolar order of most likely O_{xy}-type $(= J_x J_y + J_y J_x)$ moments coexisting with antiferromagnetic order via spin–orbit coupling in Nd $4f$ electrons.

It should be pointed out that a similar situation in the ab-plane is also recognized in the Γ_6 "two-in two-out" structure. In fact, the ferroquadrupolar interaction of $\langle O_{yz} \rangle$ and $\langle O_{zx} \rangle$ moments coexisting with planar Γ_6 and axial Γ_{10} structures and the accompanying monoclinic distortion have been revealed by resonant X-ray or neutron diffraction studies in DyB_4 and HoB_4.[28–30] The schematic view of the magnetic and quadrupolar structure has been presented in Ref. 29. These results of DyB_4, HoB_4, and NdB_4 systematically indicate that the quadrupolar interaction holds the key to what kind of structure and order parameter will be realized. Here, the frustration in the SS lattice plays an essential role in suppressing the dominance of the magnetic interaction. Namely, the emergence of the noncollinear structures is the effect of geometrical frustration, or the frustration results in quadrupoles playing a major role based on the local properties of $4f$ electrons and stabilizes not the simple Néel state but the complex order with the orthogonal structure. We think that the frustration is lifted at least partly via quadrupolar interaction. The existence of the large c-component of magnetic moments in heavy rare-earth DyB_4 and HoB_4 may result in a different quadrupole order parameter and magnetic structure from those of NdB_4.

The situation in the Γ_2 "vortex" and Γ_8 "rhombus" structures is somewhat different from that in Γ_4 and Γ_6 structures. In Γ_2 and Γ_8 structures, all the magnetic moments are parallel to the twofold axis of seven-membered boron rings and will be unfavorable for quadrupolar ordering. The Γ_8 structure has never been observed in the RB_4 series, which is consistent with our consideration that the quadrupolar interaction is a principal factor for determining the nature of structures and order parameters in the RB_4 series.

On the other hand, the Γ_2 structure has been recognized in GdB_4 and TbB_4.[35,36] GdB_4 shows the antiferromagnetic order below $T_{\mathrm{N}} = 42\,\mathrm{K}$.[15] The magnetic structure is determined to be the Γ_2-type using spherical neutron polarimetry.[35] Since Gd lacks an orbital moment ($L = 0$) and has no quadrupole moment, the magnetic anisotropy is small. However, the dipolar interaction is identified as the dominant source of magnetic anisotropy for many Gd compounds.[38] In the case of GdB_4, it is shown that the magnitude relation of the interaction energies for Γ_2 and Γ_4 structures is surely $\Gamma_2 < \Gamma_4$.[39] Thus, the emergence of the pure Γ_2 structure in GdB_4 may be the case that the magnetic dipole–dipole interaction is dominant.

For TbB_4, two antiferromagnetic transitions are identified at $T_{\mathrm{N1}} = 44\,\mathrm{K}$ and $T_{\mathrm{N2}} = 24\,\mathrm{K}$.[15] The pure Γ_2 structure is recognized in the intermediate phase ($T_{\mathrm{N2}} < T < T_{\mathrm{N1}}$) with a large moment of $7.2\,\mu_{\mathrm{B}}$, and a minor component ($\sim 30\%$) of Γ_6 is mixed into the Γ_2 structure below T_{N2}.[36] This mixing

would be interpreted as the coexistence of ferroquadrupolar ordering similar to DyB_4 and HoB_4 accompanying monoclinic distortion.[36,40] Actually, the tetragonal-to-orthorhombic distortion is determined by X-ray diffraction measurements.[41] The rotation angle of magnetic moments $\varphi \sim 23°$ in TbB_4 is more or less similar to that for NdB_4 in phase II.

So far, even if we take quadrupoles into account, isotropic exchange interactions could not lift the degeneracy of the Γ_4 and Γ_6 structures. It is also an open question why the Γ_2 structure is induced in phase II of NdB_4 even if we consider the dipolar interaction, since the mixing of the Γ_2 structure may be inconsistent with the quadrupole scenario. However, we can imagine that the underlying mechanism related to quadrupoles and frustration is in common among the RB_4 series at least with the Γ_4 or Γ_6 structure where the magnetic moments rotate 90° from the principal axis of the seven-membered ring.

The quadrupolar ordering in *f* electron systems has become familiar in recent decades even with noncubic (tetragonal) symmetry.[42–47] In most cases, the orbital as well as spin degrees of freedom (e.g., pseudo-quartet as in NdB_4) are a necessary requirement for multipole phenomena. Quadrupolar ordering in these systems can be realized when the quadrupolar interaction is sufficiently strong to overcome the magnetic interaction. This condition is very important for the pure quadrupolar order reported in DyB_2C_2.[42,43] However, we know from many examples that this favorable condition for quadrupolar ordering is rare and accidental. The successive transitions with different magnetic components such as in-plane and out-of-plane ones may be a signature for the quadrupole order parameter coexisting with the magnetic order parameter. In this case, the anisotropic magnetic interaction can cooperate with the quadrupolar interaction and, consequently, the multicomponent order parameter including quadrupoles can be stabilized by successive transitions. Despite these cooperative interactions, the quadrupolar interaction is indispensable to realize successive transitions; in the framework of the mean-field theory, it is difficult to parameterize the anisotropic interactions to stabilize the intermediate phase. The ground state will appear below the single transition point. This type of multicomponent ordering may be the origin of the component-separated magnetic ordering, reported in simple tetragonal compounds (so-called "115" system) such as $TbCoGa_5$ and $NpTGa_5$ (T = Fe, Ni, Rh).[48–55] According to this scenario, we can consider that the local *f* electron property is the most essential for the multicomponent order. At the same time, however, we can point out that the geometrical frustration effect originated from the SS lattice in RB_4 provides the condition in which the quadrupolar interaction plays an indispensable role. The magnetic structures in RB_4, which are revealed systematically from our study and previous studies, can clarify the importance of quadrupolar interaction and shed light on the emergent phenomena in *f* electron systems.

We need to further study NdB_4 by means of resonant X-ray scattering, neuron diffraction, and polarization analysis on single-crystal samples to reveal the magnetic structures and quadrupolar order parameters. Moreover, the inelastic neutron scattering study should be carried out in order to clarify the electronic state and the interaction of 4*f* electrons in this fascinating system.

5. Conclusions

We have studied the magnetic structure and the order parameter of NdB_4 with the successive phase transitions at $T_0 = 17.2\,\mathrm{K}$, $T_{N1} = 7.0\,\mathrm{K}$, and $T_{N2} = 4.8\,\mathrm{K}$ by the neutron diffraction technique. The diffraction experiments have revealed the antiferromagnetic ordering with the propagation vectors $\mathbf{q}_0 = (0,0,0)$, $\mathbf{q}_0$ and $\mathbf{q}_{s1} = (\delta,\delta,0.4)$ ($\delta \sim 0.14$), and $\mathbf{q}_0$ and $\mathbf{q}_{s2} = (0.2,0,0.4)$ in phase II ($T_{N1} < T < T_0$), phase III ($T_{N2} < T < T_{N1}$), and phase IV ($T < T_{N2}$), respectively. The magnetic structure in phase II has been uniquely determined by the group representation analysis. This structure is expressed as a linear combination of antiferromagnetic "all-in/all-out"-type (Γ_4) and "vortex"-type (Γ_2) structures, consisting of a Γ_4 main component plus a small amplitude of Γ_2. We propose that the quadrupolar order of most likely the $\langle O_{xy} \rangle$ quadrupole moments coexists with the magnetic structure of $\langle J_x \rangle$ and $\langle J_y \rangle$ in phase II, in which the quadrupolar interaction would be the dominant factor for stabilizing this noncollinear structure and quadrupolar order.

Acknowledgments

The neutron scattering experiment at Oak Ridge National Laboratory was supported in part by the U.S.–Japan Cooperative Program on Neutron Scattering. A portion of this research used resources at ORNL's High Flux Isotope Reactor was sponsored by the Scientific User Facilities Division, Office of Basic Energy Sciences, U.S. Department of Energy. This work was supported by a Grant-in-Aid for Scientific Research (C) (No. 25390133) from the Japan Society for the Promotion of Science.

*yamauchi.hiroki@jaea.go.jp

1) M. J. Harris, S. T. Bramwell, D. F. McMorrow, T. Zeiske, and K. W. Godfrey, Phys. Rev. Lett. **79**, 2554 (1997).
2) A. P. Ramirez, A. Hayashi, R. J. Cava, R. Siddharthan, and B. S. Shastry, Nature **399**, 333 (1999).
3) H. Kadowaki, Y. Ishii, K. Matsuhira, and Y. Hinatsu, Phys. Rev. B **65**, 144421 (2002).
4) Y. Shimizu, K. Miyagawa, K. Kanoda, M. Maesato, and G. Saito, Phys. Rev. Lett. **91**, 107001 (2003).
5) J. S. Helton, K. Matan, M. P. Shores, E. A. Nytko, B. M. Bartlett, Y. Yoshida, Y. Takano, A. Suslov, Y. Qiu, J.-H. Chung, D. G. Nocera, and Y. S. Lee, Phys. Rev. Lett. **98**, 107204 (2007).
6) M. Mekata and K. Adachi, J. Phys. Soc. Jpn. **44**, 806 (1978).
7) R. Brener, E. Ehrenfreund, H. Shechter, and J. Makovsky, J. Phys. Chem. Solids **38**, 1023 (1977).
8) H. Kadowaki, K. Ubukoshi, and K. Hirakawa, J. Phys. Soc. Jpn. **56**, 751 (1987).
9) B. S. Shastry and B. Sutherland, Physica B **108**, 1069 (1981).
10) H. Kageyama, K. Yoshimura, R. Stern, N. V. Mushnikov, K. Onizuka, M. Kato, K. Kosuge, C. P. Slichter, T. Goto, and Y. Ueda, Phys. Rev. Lett. **82**, 3168 (1999).
11) H. Nojiri, H. Kageyama, K. Onizuka, Y. Ueda, and M. Motokawa, J. Phys. Soc. Jpn. **68**, 2906 (1999).
12) O. Cépas, K. Kakurai, L. P. Regnault, T. Ziman, J. P. Boucher, N. Aso, M. Nishi, H. Kageyama, and Y. Ueda, Phys. Rev. Lett. **87**, 167205 (2001).
13) A. Zalkin and D. H. Templeton, Acta Crystallogr. **6**, 269 (1953).
14) Z. Fisk, A. S. Cooper, P. H. Schmtdt, and R. N. Castellano, Mater. Res. Bull. **7**, 285 (1972).
15) Z. Fisk, M. B. Maple, D. C. Johnston, and L. D. Woolf, Solid State Commun. **39**, 1189 (1981).
16) G. A. Wigger, E. Felder, R. Monnier, H. R. Ott, L. Pham, and Z. Fisk, Phys. Rev. B **72**, 014419 (2005).

17) R. Watanuki, T. Kobayashi, R. Noguchi, and K. Suzuki, J. Phys.: Conf. Ser. **150**, 042229 (2009).
18) J. Y. Kim, N. H. Sung, B. Y. Kang, M. S. Kim, B. K. Cho, and J.-S. Rhyee, J. Appl. Phys. **107**, 09E111 (2010).
19) K. H. J. Buschow and J. H. N. Creyghton, J. Chem. Phys. **57**, 3910 (1972).
20) J. Y. Kim, B. K. Cho, H. J. Lee, and H.-C. Kim, J. Appl. Phys. **101**, 09D501 (2007).
21) S. Yoshii, T. Yamamoto, M. Hagiwara, S. Michimura, A. Shigekawa, F. Iga, T. Takabatake, and K. Kindo, Phys. Rev. Lett. **101**, 087202 (2008).
22) T. Inami, K. Ohwada, Y. H. Matsuda, Z. W. Ouyang, H. Nojiri, T. Matsumura, D. Okuyama, and Y. Murakami, J. Phys. Soc. Jpn. **78**, 033707 (2009).
23) S. Yoshii, K. Ohoyama, K. Kurosawa, H. Nojiri, M. Matsuda, P. Frings, F. Duc, B. Vignolle, G. L. J. A. Rikken, L.-P. Regnault, S. Michimura, and F. Iga, Phys. Rev. Lett. **103**, 077203 (2009).
24) K. Siemensmeyer, E. Wulf, H.-J. Mikeska, K. Flachbart, S. Gabański, S. Mat'aš, P. Priputen, A. Efdokimova, and N. Shitsevalova, Phys. Rev. Lett. **101**, 177201 (2008).
25) S. Michimura, A. Shigekawa, F. Iga, T. Takabatake, and K. Ohoyama, J. Phys. Soc. Jpn. **78**, 024707 (2009).
26) K. Wierschem, S. S. Sunku, T. Kong, T. Ito, P. C. Canfield, C. Panagopoulos, and P. Sengupta, Phys. Rev. B **92**, 214433 (2015).
27) R. Watanuki, G. Sato, K. Suzuki, M. Ishihara, T. Yanagisawa, Y. Nemoto, and T. Goto, J. Phys. Soc. Jpn. **74**, 2169 (2005).
28) D. Okuyama, T. Matsumura, H. Nakao, and Y. Murakami, J. Phys. Soc. Jpn. **74**, 2434 (2005).
29) D. Okuyama, T. Matsumura, T. Mouri, N. Ishikawa, K. Ohoyama, H. Hiraka, H. Nakao, K. Iwasa, and Y. Murakami, J. Phys. Soc. Jpn. **77**, 044709 (2008).
30) T. Matsumura, D. Okuyama, T. Mouri, and Y. Murakami, J. Phys. Soc. Jpn. **80**, 074701 (2011).
31) J. Rodríguez-Carvajal, Physica B **192**, 55 (1993).
32) A. S. Wills, Physica B **276–278**, 680 (2000).
33) A. S. Wills, Phys. Rev. B **63**, 064430 (2001).
34) K. Momma and F. Izumi, J. Appl. Crystallogr. **44**, 1272 (2011).
35) J. A. Blanco, P. J. Brown, A. Stunault, K. Katsumata, F. Iga, and S. Michimura, Phys. Rev. B **73**, 212411 (2006).
36) T. Matsumura, D. Okuyama, and Y. Murakami, J. Phys. Soc. Jpn. **76**, 015001 (2007).
37) W. Schäfer, G. Will, and K. H. J. Buschow, J. Chem. Phys. **64**, 1994 (1976).
38) M. Rotter, M. Loewenhaupt, M. Doerr, A. Lindbaum, H. Sassik, K. Ziebeck, and B. Beuneu, Phys. Rev. B **68**, 144418 (2003).
39) D. C. Johnston, Phys. Rev. B **93**, 014421 (2016).
40) D. Okuyama, Dr. Thesis, Faculty of Science, Tohoku University, Sendai (2007) [in Japanese].
41) Z. Heiba, W. Schäfer, E. Jansen, and G. Will, J. Phys. Chem. Solids **47**, 651 (1986).
42) Y. Tanaka, T. Inami, T. Nakamura, H. Yamauchi, H. Onodera, K. Ohoyama, and Y. Yamaguchi, J. Phys.: Condens. Matter **11**, L505 (1999).
43) K. Hirota, N. Oumi, T. Matsumura, H. Nakao, Y. Wakabayashi, Y. Murakami, and Y. Endoh, Phys. Rev. Lett. **84**, 2706 (2000).
44) K. Ohoyama, H. Yamauchi, A. Tobo, H. Onodera, H. Kadowaki, and Y. Yamaguchi, J. Phys. Soc. Jpn. **69**, 3401 (2000).
45) T. Yanagisawa, T. Goto, Y. Nemoto, S. Miyata, R. Watanuki, and O. Suzuki, Phys. Rev. B **67**, 115129 (2003).
46) K. Kaneko, H. Onodera, H. Yamauchi, T. Sakon, M. Motokawa, and Y. Yamaguchi, Phys. Rev. B **68**, 012401 (2003).
47) A. M. Mulders, U. Staub, V. Scagnoli, Y. Tanaka, A. Kikkawa, K. Katsumata, and J. M. Tonnerre, Phys. Rev. B **75**, 184438 (2007).
48) N. Sanada, R. Watanuki, K. Suzuki, M. Akatsu, and T. Sakakibara, J. Phys. Soc. Jpn. **78**, 073709 (2009).
49) Y. Tokunaga, Y. Saito, H. Sakai, S. Kambe, N. Sanada, R. Watanuki, K. Suzuki, Y. Kawasaki, and Y. Kishimoto, Phys. Rev. B **84**, 214403 (2011).
50) A. Kiss and Y. Kuramoto, J. Phys. Soc. Jpn. **75**, 034709 (2006).
51) N. Metoki, J. Phys. Soc. Jpn. **75** [Suppl.], 24 (2006).
52) S. Jonen, N. Metoki, F. Honda, K. Kaneko, E. Yamamoto, Y. Haga, D. Aoki, Y. Homma, Y. Shiokawa, and Y. Ōnuki, Phys. Rev. B **74**, 144412 (2006).
53) F. Honda, N. Metoki, K. Kaneko, S. Jonen, E. Yamamoto, D. Aoki, Y. Homma, Y. Haga, Y. Shiokawa, and Y. Ōnuki, Phys. Rev. B **74**, 144413 (2006).
54) S. Kambe, H. Sakai, Y. Tokunaga, R. E. Walstedt, D. Aoki, Y. Homma, and Y. Shiokawa, Phys. Rev. B **76**, 144433 (2007).
55) A. Kiss and Y. Kuramoto, J. Phys. Soc. Jpn. **77**, 124708 (2008).